Vibration control of offshore wind turbine under multiple hazards using single variable-stiffness tuned mass damper

Dingxin Leng, Yi Yang, Kai Xu, Yancheng Li, Guijie Liu*

Abstract: With high flexibility and low damping, offshore wind turbines (OWT) are prone to external vibrations such as wind, sea waves and earthquake, either attacked individually or as combined loading cases. This study proposes a semi-active variable-stiffness tuned mass damper (VSTMD) with magnetorheological elastomer (MRE) materials to mitigate undesired dynamic responses of OWT. A jacket-supported OWT with VSTMD installed on top of the tower is adopted as an example to demonstrate the effectiveness of the proposed design under single hazard and multiple hazards. A semi-active frequency tracing algorithm is proposed through which the current-dependent stiffness of MRE-TMD is controlled by tracking the acceleration of OWT tower. The numerical results demonstrate that the semi-active MRE-VSTMD can effectively attenuate the dynamic responses of OWT under multi-hazard loadings, and it outperforms the passive TMD in reducing the peak and RMS displacement of tower structure. Robustness analysis of semi-active VSTMD is also validated by considering OWT stiffness decay under multiple-loadings.

Keywords: Offshore wind turbine, vibration control, tuned mass damper, magnetorheological elastomer.

1. Introduction

Offshore wind turbines (OWTs) are paid increasingly attention as desirable choice of clean energy production. In practical, various OWTs are available, e.g. monopiles and gravity-foundation type in shallow water depth (0-20 m), jacket-supported, tripods and trusses in transitional water depth (40-60 m), and floating structures in deep water (60-120 m) [书 1-Ref.1]. With the development of new material, OWT with large rotor and slender tower can e achieved in the design process. For example, in a latest NREL 5WM OWT structure, rotor diameter is 126 m and the tower height is 87.6 m with the maximum wall thickness of 0.027 m [书 1-Ref.2]. These thin-walled structures have high flexibility and low damping ratio (e.g. 1% to 1.5% [书 3]), which are vulnerable to external excitation (e.g. wind and wave loadings). In some hostile environments such as seismic prone area [1], OWT may also suffer violent seismic loadings, which could cause excessive vibration responses. The vibrations in offshore wind turbine would compromise the energy production and lead to structural failure [2, 3].

During last decades, extensive researches have been conducted to mitigate the vibration of OWT structures under multiple-hazard loadings. Many devices have been proposed and utilized for this purpose such as tuned liquid dampers (TLDs) [??], tuned liquid column dampers (TLCDs) [??], tuned mass dampers (TMDs), frictional dampers [??] and viscoelastic or viscos-fluid dampers [??]. Among these, TMD is generally considered as a suitable and feasible method to control OWT dynamic responses due to its effectiveness, robustness and easy-installation. In principle, TMD is an auxiliary spring-damper-mass system adhered to the primary wind turbine structure which resonates out of phase with targeted structure, and hence a large amount of vibrating energy from the main structure is transferred and dissipated. For offshore wind turbines in coastal area, combined wind and wave loadings are assumed as the major external excitations. The energies of wind/wave loadings are concentrated in a low frequency range (e.g. below 0.1Hz in wind and less than 0.2 Hz in wave [4]), which normally excites the first vibration mode of OWT tower (e.g. 0.31 Hz in jacket type [5], 0.27Hz monopile type [6-8]). In this case, it is reasonable to utilize one TMD device in the OWT nacelle, and the TMD's design parameters normally target the fundamental frequency of OWT. Some related researches have been conducted [书 2-Ref8-Ref10] and the vibration mitigation effects were confirmed.

However, earthquake is another vibration excitation to be considered as the coastal areas where the OWTs are usually placed are also seismic prone regions. It is known that seismic energy has a broader frequency range with dominant energy in the range of 0.7 Hz ~ 3.0 Hz [11], which may excite high vibration modes of OWT structure (e.g. 1.19 Hz in 2nd frequency of jacket OWT [5]). Consequently, for the worst scenarios (e.g., under actions of wind, wave and earthquake), the first two vibration frequencies of OWT may be simultaneously excited. In this case, one TMD device designed for the fundamental frequency of OWT in wave/wind loadings may be not be effective. Therefore, a multiple TMDs (MTMD) design was proposed, in which each TMD was set to deal with one single vibration frequency. Zuo et al [12] developed a series of MTMD along the OWT tower. Their results showed that MTMD system could reduce dynamic responses in different vibration modes. Hussan et al. [5] proposed two TMDs at the top and bottom of the tower respectively to mitigate vibration modes of one jacket-support OWT in combined seismic and wind excitations. However, MTMD system would induce large installation and maintain costs [15]. In addition, these passive TMD and MTMD are very sensitive to tuning frequency ratio, even when optimally designed [6]. It is proved that a difference of 1.5% in frequency match to the primary structure leads to 70% deterioration in

the vibration mitigation effect [Wind-induced vibration control of a constructing bridge tower with MRE variable stiffness tuned mass damper].

Compared with passive devices, semi-active TMD possessing variable stiffness provides a solution to vibration control of OWT since the variable-stiffness semi-active TMD is able to trace the varying excited frequency of OWT in real time under multi-hazards loadings. In particular, as there is only one single semi-active TMD required, the implementation costs could be substantially reduced in comparison with MTMD [15]. Dinh et al [Semi-active control of vibrations of spar type floating offshore wind turbines] conducted an analysis of semi-active TMD for vibration control of spar type offshore wind turbines. Its effectiveness was evaluated and validated under time-varying mooring cable tension, rotor speed and the blade stiffness of OWT structure. Hemmati et al [书 1-92 页] proposed a semi-active TMD for structural control of 5 MW NREL wind turbine, and the numerical results demonstrated the proposed semi-active TMD could mitigate the time-variant vibration responses under different wind, sea wave and seismic excitations. Sun et al [16, 书 2-24 页] developed a semi-active TMD with variable stiffness to control monopile OWT subjected to multi-hazards (e.g. wind, wave and earthquake). With considering damage effects, retuned real-time STMD still presented consistent effectiveness when the dominant frequency of OWT was changeable.

The main contribution of the present work is to propose a variable-stiffness TMD in the semi-active vibration control of an offshore wind turbine under multiple-hazards loadings using smart MRE materials. Magnetorheological elastomer (MRE), a smart elastomeric composite, can adjust its elastic modulus or stiffness by altering external magnetic field and then immediately revert to its initial status when the field is removed. Recent studies demonstrate that MRE is a potential candidate to semi-active variable-stiffness TMD [17-20]. Although the potential of MRE-base structure for vibration control has been presented [21], the application of MRE-base device in ocean engineering has not been reported.

To this end, a jacket-up offshore wind turbine is adopted as a case study. Multiple degree-of-freedom (DOF) modelling of OWT is established by the dynamic finite element method. For semi-active control, a real-time frequency trace algorithm is proposed. The vibration control effectiveness is comprehensively evaluated and validated, and the robustness of the control algorithm is also discussed. The structure of this paper is organized as follows. Section 2 introduces the structural model of offshore wind turbine excited by multiple hazard loadings. Design and working principles of variable stiffness MRE-TMD for vibration control of OWT are proposed in Section 3. Numerical simulation results of vibration mitigation of OWT-MRE-

TMD system are discussed in Section 4, and its semi-active robustness is also evaluated. Main conclusions are drawn in Section 5.

2. Structural model

2.1 NREL 5MW offshore wind turbines

Jacket-supported OWT is a commonly structure to enable large-scale implementation of offshore wind farms in transitional water depth (in the range of 40 m to 60 m) [**]. In the present work, the studied case is NREL 5MW jacket supported offshore wind turbine [22-24, 3 篇 5MW 导管架风机为对象的论文], as shown in Figure 1. This OWT structure is divided into five parts: nacelle and blades, tower, transition piece (TP) and jacket base structure, [25 模型参数 Fabian et al, 2011, (国外硕士论文)]. The length of each blade is 61.5 m and the rotor radius is 63 m. The hub height is 90.55 m above mean sea level (MSL) and the hub vertical offset is 2.4 m. The conical tower has a total length of 68 m. The TP is a rigid concrete block with a mass of 666 ton, located at the top of the jacket and the bottom of the TP is at 16.15m, the height of the concrete transition piece is 4m, which sets the interface level at 20.15m.

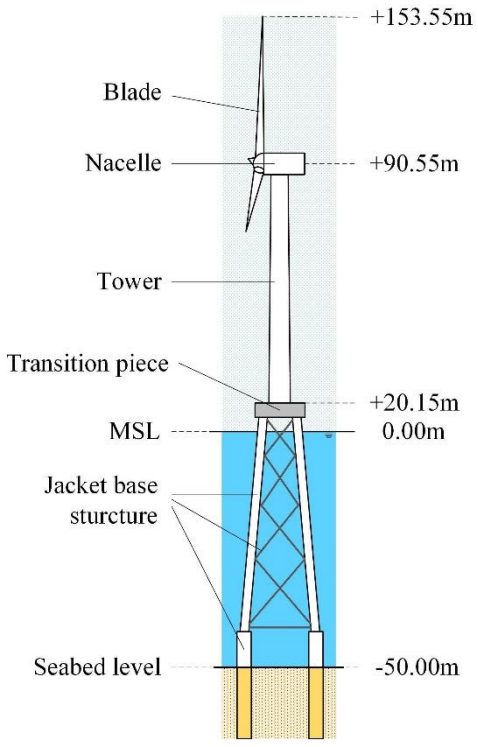

Figure 1. Configuration dimensions and components of OWT system

The structural parameters [26 Hemmati A et al, 2019] of the jacket supported wind turbine are listed in Table 1. Damping ratio is adopted as 1%, excluding aerodynamic damping.

Table 1. Details of NREL-5MW jacketed supported OWT

Rating	5MW
Rotor Orientation	Upwind, 3 Blades
Rotor, Hub Diameter	126m, 3m
Hub Height	90.55m
Cut-In, Rated, Cut-Out Wind Speed	3 m/s, 11.4 m/s, 25m/s
Cut-In, Rated Rotor Speed	6.9rpm, 12.1rpm
Rotor Mass	110,000kg
Nacelle Mass	240,000kg
Tower Mass	260,000kg
Transition Piece	4m*9.6m*9.6m

2.2 Numerical model and validation

To investigate the dynamic responses of wind turbine, a finite element model of NREL 5MW jacket supported OWT is established, as shown in Figure 2. The wind and wave loadings are calculated and applied to tower and jacket nodes as nodal force and moments, and seismic loading is applied by inertia effect of individual element. The established jacket is made of 4 central piles, 4 levels of X-braces, mud braces four legs and a transition piece (TP). The tower is cone bucket structure, and its material properties are listed in Table 2.

Table 2. Material properties of tower structure

Young's Modulus (GPa)	Poisson Ratio	Density(kg/m3)
210	0.3	7850

The rotor nacelle assembly (RNA) is considered as lumped mass at the top of the tower [5] (Figure 2), and the influence of the geometries of the nacelle and blades is not considered. Such simplification is reasonable as the rotation of the blades mainly affected the blades themselves and has less effect on the OWT main structure (e.g. tower and jacket support structure) [29]. Please note that the scope of this paper limits at the parked condition of OWT, in which the dominant wind loading is the wind applied on OWT tower and nacelle, not blades assembles [3]. The TP is assumed as a rectangular rigid body [5]. In addition, soil-structure interaction (SSI) is not considered, and six-times of pipe diameter is applied at ground level to simulate the soil-structural boundary condition. This might slightly change the optimal frequency and

damping parameter of designed TMD, yet the effectiveness evaluation of vibration mitigation in OWT-TMD system is not compromised [3].

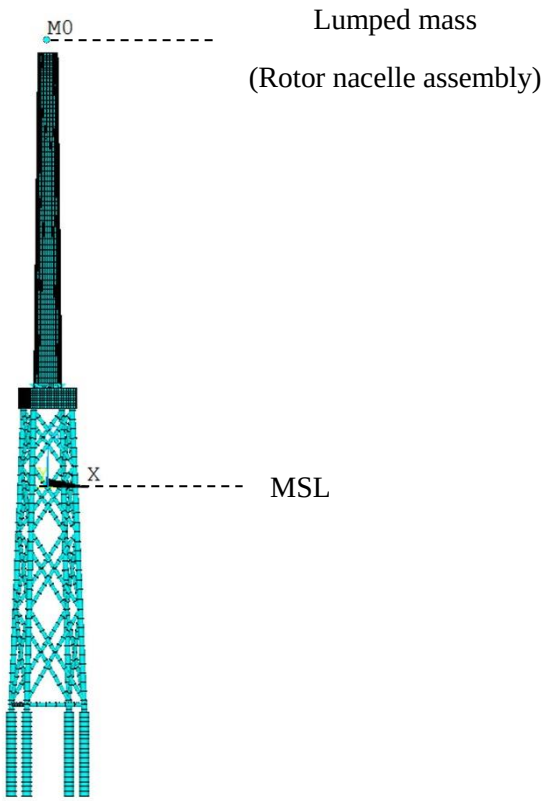

Figure 2. Jacket supported 5MW offshore wind turbine model

Figure 3 illustrates the mode shapes of OWT structure and its natural frequencies are calculated in Table 3. In the first two vibration modes, offshore wind turbine vibrates orthogonally in side and for-aft directions. The obtained natural frequency of finite element model has been assimilated with the original reference model [25-国外硕士论文].

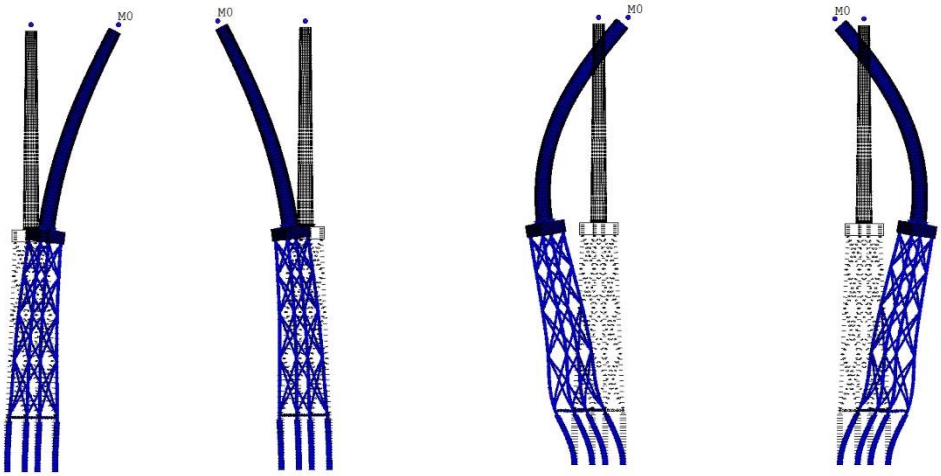

(a) (b) (c) (d)

Figure 3. Mode shape of the ANSYS FEM:

(a) first side-side, (b) first fore-aft, (c) second side-side, (d) second fore-aft.

Table 3. Natural frequencies (Hz) of the numerical model

Mode shape	Finite element method	Original structure analysis [25]
First slide-slide	0.3153	0.3190
First fore-aft	0.3153	0.3190
Second slide-slide	1.1090	1.1944
Second fore-aft	1.1090	1.1944

2.3 Multiple hazard loadings

2.3.1 Wind load

Wind loading is consisted of a constant mean wind and a fluctuating component. The wind velocity is expressed as follows,

$$V(z,t)=\bar{v}(z)+v(z,t) \tag{1}$$

where $\bar{v}(z)$ is the average wind velocity at height z, and $v(z,t)$ is the fluctuating wind velocity at height z.

In practical, the wind velocity at a specific height should be firstly selected as a reference point (e.g. the height of nacelle is chosen as the reference), and the wind speed at different height, $\bar{v}(z)$, is obtained according to the wind speed relationship as shown in Eq.(2) [30-[DNV, 2004]]

$$\bar{v}(z)=\bar{v}_{ref}\frac{\ln\left(\frac{z}{z_0}\right)}{\ln\left(\frac{z_{ref}}{z_0}\right)} \tag{2}$$

where v_{ref} is the mean wind velocity at height z_{ref}; $\bar{v}(z)$ is the mean wind velocity in any height z; z_{ref} is the reference height, and it is 90.55 m in the present work; z_0 is surface roughness length parameter.

The Davenport spectrum [31,3211,12] is utilized to model the power spectral density (PSD) function of the fluctuating wind velocity, expressed as follows

$$S_v(n)=4k\bar{v}_{10}\frac{x^2}{n(1+x^2)^{4/3}} \tag{3}$$

in which $S_v(n)$ is wind power spectral density function; n is fluctuating frequency; $x=\frac{1200n}{\bar{v}_{10}}$; $\bar{v}_{10}$ is the mean wind velocity at 10 m above the sea surface; k is the surface roughness length.

The spatial correlation effect is used to capture the common features of the wind loads along the wind turbine tower. In the present work, this effect is described by a spatial coherency function, *Coh*(*w*), [33,3413,14]

$$Coh(\omega)=\exp(-\frac{\omega\sqrt{C_z^2\left(z_i-z_j\right)^2}}{2\pi\hat{V}}) \tag{4}$$

in which, ω is the circular frequency of wind velocity; C_z is the a dimensionless attenuation coefficient; $\hat{V}$ is the mean wind velocity first between i th point and j th point.

Considering the influence of spatial correlation effect, the correlation power spectrum density function of fluctuating wind velocity in space can be obtained as,

$$S_{ij}\left(\omega\right)=\sqrt{S_{ii}\left(\omega\right)S_{jj}\left(\omega\right)}Coh\left(\omega\right) \tag{5}$$

in which $S_{ii}\left(\omega\right)$ and $S_{jj}\left(\omega\right)$ represent the power spectrum of the fluctuating wind at location i and j respectively. $S_{ij}\left(\omega\right)$ represents the power spectrum between points i and j.

Fast Fourier transform (FFT) is introduced here based on the harmonic superposition method to simulate the stochastic process of fluctuating wind velocity. The periodic spectral density function matrix is

$$\underline{S}\left(\omega\right)=\begin{pmatrix}S_{11}\left(\omega\right) & \cdots & S_{1n}\left(\omega\right)\\ \vdots & \ddots & \vdots\\ S_{n1}\left(\omega\right) & \cdots & S_{nn}\left(\omega\right)\end{pmatrix} \tag{6}$$

where $S_{ij}\left(\omega\right)\left(j=1,2,...,n;k=1,2,...,n\right)$ is the Fourier transform of the relevant function, $\underline{S}\left(\omega\right)$ can be decomposed into

$$\underline{S}\left(\omega\right)=H\left(\omega\right)\cdot H^{*}\left(\omega\right)^{T} \tag{7}$$

where, $H\left(\omega\right)$ is the lower triangular matrix, and the fluctuating wind velocity form to be simulated is

$$V\left(t\right)=\sum_{k=1}^{j}\sum_{l=1}^{N}\left|H_{jk}\left(\omega_{kl}\right)\right|\sqrt{2\Delta\omega}\cos\left(\omega_{kl}t+\theta_{kl}\right)\left(j=1,2,...,\mathrm{n}\right) \tag{8}$$

in which θ_j is a random variable evenly distributed variable in $(0, 2\pi)$. $\Delta\omega$ is frequency increment, $\Delta\omega = (\omega_n - \omega_k)/n$; ω_k is the starting point of frequency; ω_n is the end point of frequency, N is the sampling point of frequency.

The total wind loading acted on the offshore wind turbine is composed of a mean and a fluctuating component as [35-16]

$$F_i(t) = \bar{f}_i + f_i \tag{9}$$

in which the mean nodal wind load, $\bar{f}_i$ is expressed as

$$\bar{f}_i = 0.5 C_d A \rho \bar{v}_i^2 \tag{10}$$

and the fluctuating nodal wind load, f_i, is

$$f_i = C_d A \rho \bar{v}_i v_i \tag{11}$$

where the C_d is the coefficient of drag, ρ is the density of air, A is the windward area of the tower, $\bar{v}_i$ and v_i is the mean and fluctuating wind velocity of point i respectively.

The high wind velocity at hub height is 42.73 m/s in parked wind turbine. Figure 4 shows the wind velocity PSDs and the corresponding model values. The model and simulated coherency loss functions between tower top and base is shown in Figure 5. It is observed that the model and simulated values are matched well. Figure 6 shows the time history of total wind loading applied on the top and base of the OWT tower.

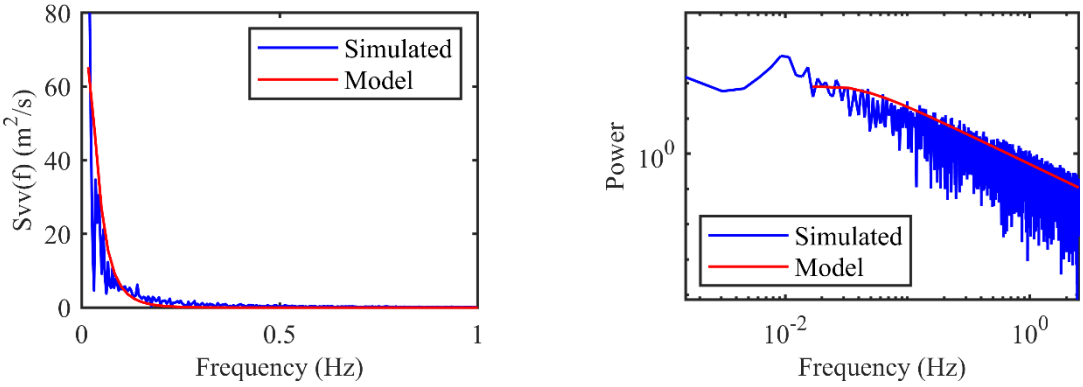

Figure 4. Comparisons of wind velocity (a) PSD and (b) coherency loss between tower top and base

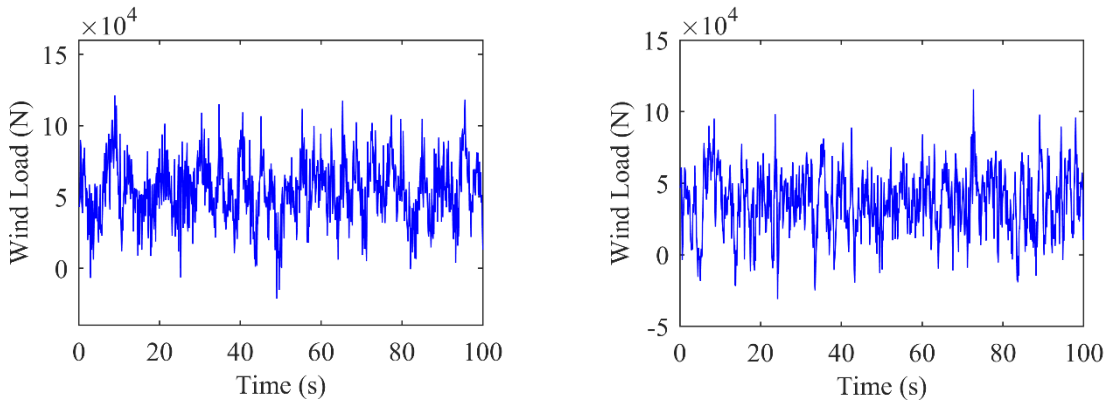

(a) (b)

Figure 5. Total wind loads: (a) for the top and (b) for the base

2.3.2 Wave load

Sea wave is a typical random process, and the energy distribution of the constituent waves can be described by wave spectrum. The commonly used wave spectrum includes frequency spectrum and direction spectrum. The JONSWAP spectrum is utilized to simulate the wave elevation, shown as follows

$$S_{\eta\eta}(f)=\frac{\alpha g^2}{\omega^2}\exp\left[-\frac{5}{4}\left(\frac{\omega_m}{\omega}\right)^4\right]\gamma^{\exp\left[-\frac{(\omega-\omega_m)^2}{2\sigma^2\omega_m{}^2}\right]} \tag{12}$$

in which, η is the sea surface elevation; γ is the peak enhancement factor (here we adopted 3.3 in this paper); g is gravitational acceleration; σ is the peak shape factor is

$$\begin{cases}\omega\le\omega_m,\sigma=0.07\\ \omega>\omega_m,\sigma=0.09\end{cases} \tag{13}$$

The spectrum is improved as [Goda (36-1999)], [*Wave mechanics for ocean engineering*(王树青《海洋工程波浪力学》)]

$$S_\eta(\omega)=\alpha^* H_s{}^2\frac{\omega_m{}^4}{\omega^5}\exp\left[-\frac{5}{4}\left(\frac{\omega_m}{\omega}\right)^4\right]\gamma^{\exp\left[-\frac{(\omega-\omega_m)^2}{2\sigma^2\omega_m{}^2}\right]} \tag{14}$$

in which, the constant α^* in this equation is

$$\alpha^*=\frac{0.0624}{0.230+0.0336\gamma-0.185(1.9+\gamma)^{-1}} \tag{15}$$

The sea surface elevation $\eta(t)$ can be expressed as

$$\eta(t)=\sum_{i=1}^{n}\sqrt{2d\omega S_{\eta\eta}(\omega_i)}\cos\left(\omega_i t+\varphi_{nn}(\omega_i)\right) \tag{16}$$

where the $\varphi_{nn}(\omega_i)$ is random phase angles and at the range of $[0, 2\pi]$.

The velocity and acceleration of water particles in the horizontal direction can be calculated by [12]

$$v_x = \frac{H\omega}{2}\frac{\cosh k(d+z)}{\sinh kd}\cos(kx-\omega t+\varphi) \tag{17}$$

$$a_x = \frac{\partial v_x}{\partial t} = \frac{H\omega^2}{2}\frac{\cosh k(d+z)}{\sinh kd}\cos(kx-\omega t+\varphi) \tag{18}$$

In present study, equal frequency method and Morison equation will be used to calculate the sea wave force. The wave force of dz length at the height z of the jacket leg is shown as

$$dF_H = f_H dz = \frac{1}{2}C_D\rho v_x|v_x|dz + C_M\rho\frac{\pi D^2}{4}a_x dz \tag{19}$$

in which C_D and C_M are the drag and inertia coefficients respectively, in this paper, $C_D = 0.65$, $C_M = 2$; $\rho = 1030\ \mathrm{kg/m^3}$ is the sea water density.

The sea state is adopted as wave height, $H_s = 9.4\ \mathrm{m}$, $T = 10.47\ \mathrm{s}$, $d = 50\ \mathrm{m}$. The PSD of the simulated sea surface elevation is shown in Figure 6, and the sea wave force acted the wind turbine structure above the mean sea level is shown in Figure 7.

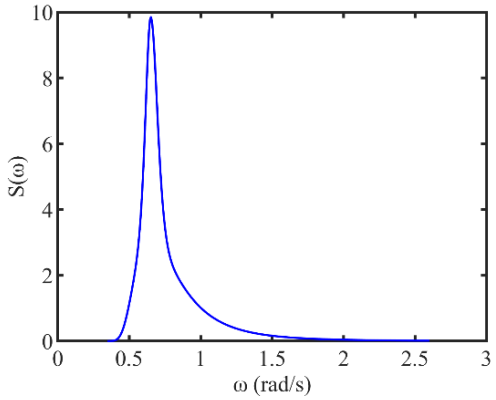

Figure 6. Frequency spectrum of wave load

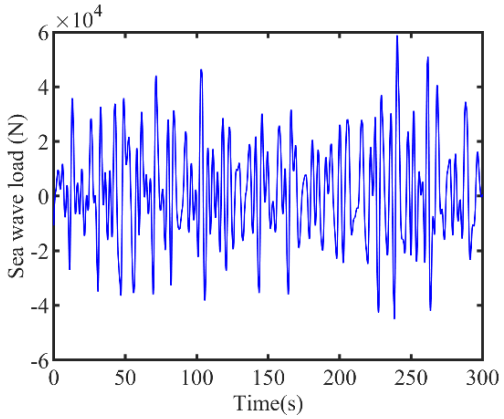

Figure 7. Sea wave load time history of 5th DOF

2.3.3 Seismic loadings

In earthquake prone areas, seismic loading may be a major environmental load for offshore wind turbine. In previous work on OWT under seismic loading, several typical earthquakes are utilized, such as Kobe, Taft, El-Centro NS, Hachionhe, etc. In the present work, two types of seismic loading are utilized, such as far-fault earthquake (EI-Centro 1940) featuring wider frequency range and last longer excitation time, and near-fault earthquake waveforms (Kobe 1995) containing large velocity pulses with lower frequency [37-]. Figure 8 represents the time history of acceleration and frequency response spectra.

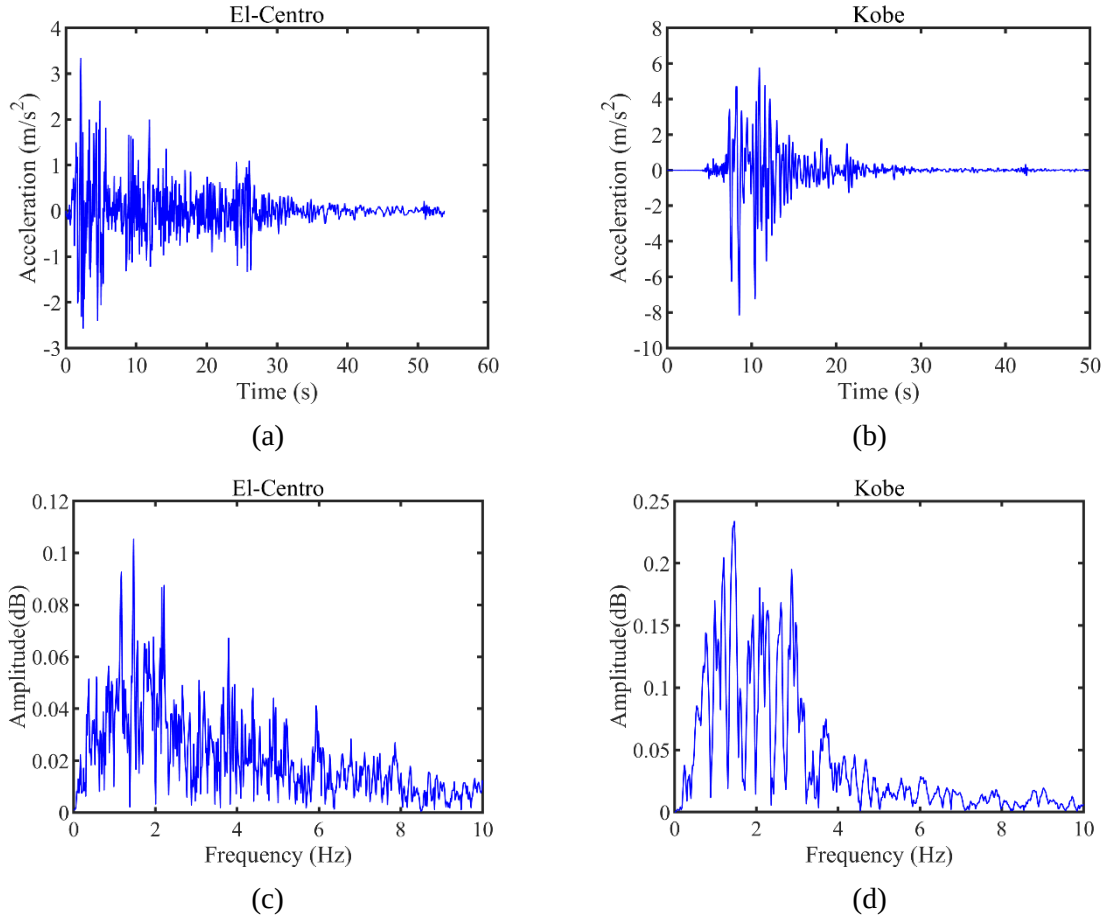

Figure 8. Seismic loadings: (a) time history of El-Centro, (b) time history of Kobe, (c) frequency response spectra of El-Centro, (d) frequency response spectra of Kobe.

3. Variable stiffness TMD

The semi-active variable stiffness tuned mass damper (VSTMD) was initially proposed by Nagarajaiah and Varadarajan [38, 39-!2005-engineering structure-variable stiffness-15, 22]. The VSTMD has a single mass with variable stiffness spring and a damping component, which has the distinct capacity of continuously retuning its frequency in real time. Figure 9 schematically shows the varied stiffness range of VSTMD.

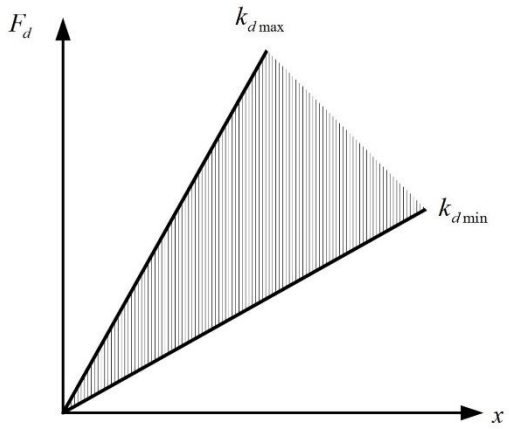

Figure 9. Characteristics of VSTMD.

3.1 Variable stiffness MRE-TMD

In the present work, a multiple-layer MRE-TMD is utilized for semi-active vibration control of OWT, as shown in Figure 11. It is consisted of an MRE isolator connected to a mass block. An enclosed magnetic path is formed composed of steel plates, MRE and coil components as shown in the red arrow. The lateral stiffness of the device can be adjusted to be more than 10 times higher when sufficient magnetic field is provided to energize the MRE materials. In the device, the magnetic field is generated by an electromagnetic coil with input current.

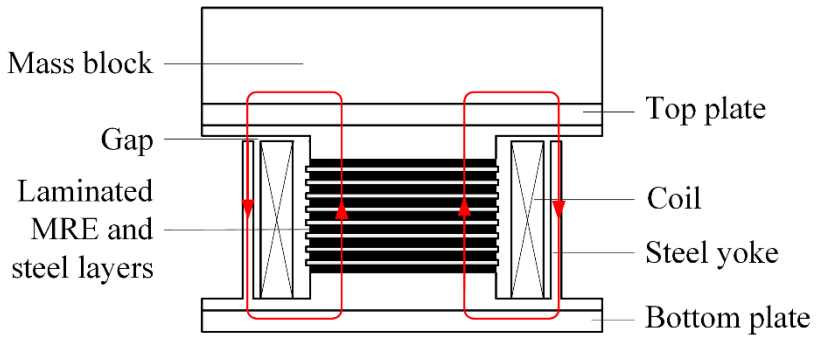

Figure 11. Design of MRE-TMD system

An MRE isolator fabricated by Li et al [43] is utilized in the present work. The current-dependent hysteresis performance of the MRE isolator is shown in Figure 12. With the variation of the applied current, the stiffness of MRE device (the slope of force-displacement) is changeable, which provides the possibility for variable stiffness TMD. The nonlinear current-dependent properties can be expressed by the following equations [44],

$$k_0(I) = a_1 \cdot I + a_0 \tag{20}$$

$$c_0(I) = b_2 \cdot I^2 + b_1 \cdot I + b_0 \tag{21}$$

$$\alpha(I) = c_2 \cdot I^2 + c_1 \cdot I + c_0 \tag{22}$$

where $k_0(I)$, $c_0(I)$ and $\alpha(I)$ are all functions related to current I, which represent the stiffness, damping and the coefficient of the strain-stiffening component. The values of coefficients $a_0, a_1, b_0, b_1, b_2, c_0, c_1, c_2$ are referred by Li et al's work [44].

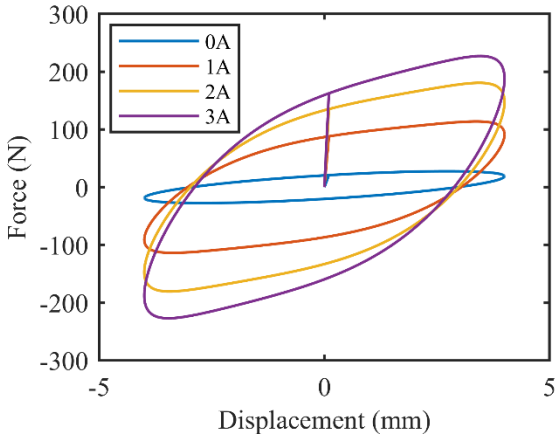

Figure 12. Current-dependent hysteresis performance of MRE isolator.

Under multi-hazard loadings, the first two vibration modes of OWT structure are likely to be excited; thus the corresponding natural frequency range of these two modes are the targeted vibration suppression for MRE-TMD system. Referred to Wang's work [Motion Control of …], the optimal frequency ratio is set as $\lambda_{opt} = \frac{(1+0.5\mu)^{\frac{1}{2}}}{(1+\mu)}$. Consequently, the resonance frequency range of MRE-TMD system is targeted as $\left[\lambda_{opt} \cdot f_1, \lambda_{opt} \cdot f_2\right]$, where f_1 and f_2 correspond to the first and second natural frequency of offshore wind turbine structure as shown in Section 2.2. The desired real-time stiffness of MRE-TMD system is calculated as $k_{TMD} = 4\pi^2 f_i^2 m_{TMD}$ where f_i is the frequency in the excited resonance frequency range of OWT structure. It is known that the mass ratio of TMD device is normally designed to be from 1% to 8% [45]. For optimal vibration mitigation effectiveness, the mass ratio of MRE-TMD by OWT structure is adopted as 5% in this paper [46].

Following the above design principle, the mass of designed TMD is 1.41×10^5 kg and the variable stiffness of MRE isolator in TMD system is in the range of 6.11×10^5 N/m and 7.39×10^6 N·m. It should be noted that the proposed MRE isolator is a much larger version of the device shown in Figure 12 with similar stiffness variable functional range e.g. 1630%. The magnified mechanical parameters of MRE isolator are then obtained. Considering the vibration

mitigation effectiveness and space limit, semi-active variable stiffness MRE-TMD is installed in the nacelle.

3.2 Semi-active frequency-tracing control algorithm

Dynamic equation of the offshore wind turbine with MRE-VSTMD system under multi-hazard loadings is shown in Eq. (1).

$$[M]\{\ddot{x}\}+[C]\{\dot{x}\}+[K]\{x\}=[B]\{F(\mathrm{t})\}+[D]\{F_{MRE-TMD}\} \tag{23}$$

where $\{x\}$, $\{\dot{x}\}$, $\{\ddot{x}\}$ are the unknown displacement, velocity and acceleration vectors respectively; $[M],[C],[K]$ are mass, damping and stiffness matrices of the OWT structure with order P (the degrees of freedom of the OWT structure). The damping matrix $[C]=\alpha[M]+\beta[K]$ is obtained using Reyleigh's damping ratio in vibration modes. $\{F(\mathrm{t})\}$ is the external loads matrix and $\{F_{MRE-TMD}\}$ is the force vector which represents the control force generated by MRE-TMD system, $[B]$ and $[D]$ matrices are their location vectors.

In practical, high acceleration of the tower top can induce mechanical malfunctioning of acceleration sensitive parts in the nacelle (e.g. gear box and generator). Hence, the acceleration in tower top is chosen as tracing index. Short-time Fourier transform (STFT) algorithm is adopted as the real-time control algorithm to identify the time-frequency characteristics of non-stationary signals [6]. Taking the acceleration signal $x(\tau)$ of tower top as the objective, its weighted signal, $\hat{x}(\tau)$ can be constructed by multiplying a window function $h(\tau-t)$,

$$\hat{x}(\tau)=x(\tau)h(\tau-t) \tag{24}$$

in which $\hat{x}(\tau)$ is a weighted signal, t is the fixed time, and τ is the running time.

Applying Fourier transformation to the weighted signal, the spectrum $X(t,\omega)$ can be obtained,

$$X(t,\omega)=\frac{1}{2\pi}\int e^{-j\omega t}\hat{x}=\frac{1}{2\pi}\int e^{-j\omega t}x(\tau)h(\tau-t) \tag{25}$$

The power spectral density $P(t,\omega)$ at time t is as follows,

$$P(t,\omega)=\left|X(t,\omega)\right|^2=X(t,\omega)\cdot\overline{X(t,\omega)} \tag{26}$$

At the fixed time t_i, the dominant frequency ω_{id} is calculated by Eqs.(**) and (**),

$$\omega_i=\left\{\omega\,|\,P(t_i,\omega)=\max\left\{P(t_i,\omega)\right\}\right\} \tag{27}$$

$$\omega_d = \frac{\sum_{k=\max\{1,i=m+1\}}^{i} \omega_i(t_k)\max\{P(t_k,\omega)\}}{\sum_{k=\max\{1,i-m+1\}}^{i} \max\{P(t_k,\omega)\}} \tag{28}$$

where ω_i is the instantaneous frequency, and ω_d is the dominant frequency at t_i calculated through averaging the values of the instantaneous frequencies over m time steps.

The flow chart of real-time tuning strategy is shown in Figure 13. The acceleration response of tower top is measured and the response frequency is identified by STFT; the targeted natural frequency of MRE-TMD device is then determined and the stiffness of MRE-TMD to trace the real-time response frequency is obtained; using Eq (20), the desirable control current can be obtained.

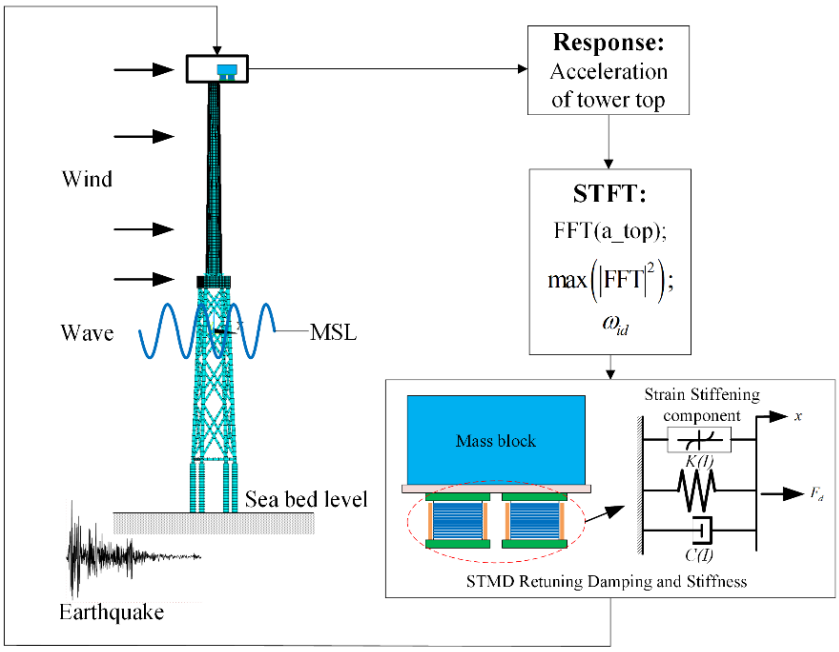

Figure 13. Semi-active control of variable stiffness MRE-TMD

4. Results and discussions

4.1 Model verification with MRE-TMD system

Sweep acceleration signal is utilized to verify the effectiveness of MRE-TMD device in the structure over a wide frequency range. The frequency chosen is between 0.01-10Hz and a maximum PGA 1.012 g is reached in 200 seconds with an equal spacing of 0.01 sec. Figure 14 shows the amplitude of the accelerations in the top and base of the tower under uncontrolled, passive, and semi-active control variable stiffness MRE-TMD system. It is noted that passive

system used in this paper refers to a system with MRE-TMD at zero current. For continence, we use the term of passive TMD throughout the paper.

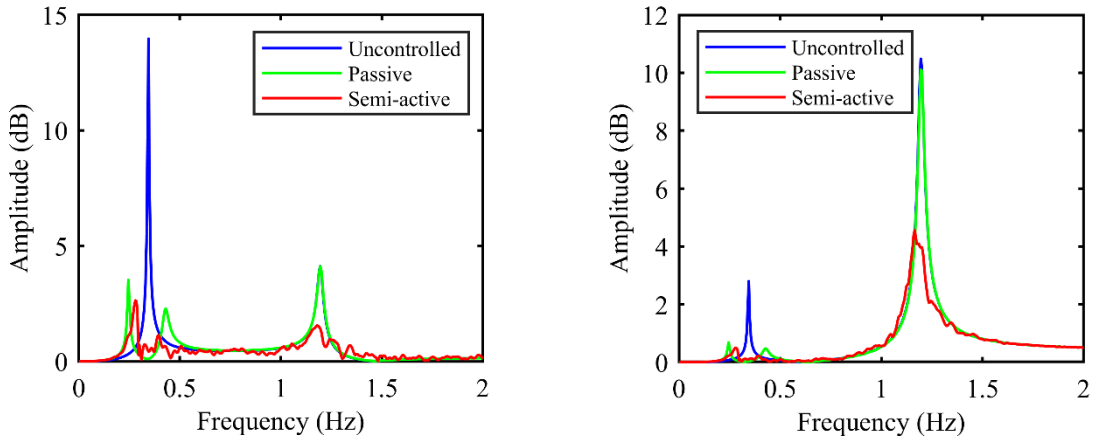

Figure 14. Response spectra: (a) for the top; (b) for the base

As shown in Figure 14, the OWT structure is excited at the first two fundamental natural frequencies under sweep frequency loading. In terms of vibration mitigation, passive TMD performs effective only at the first mode. However, semi-active MRE-TMD can track the acceleration response frequency with variable stiffness, and both first and second vibration modes can be effectively mitigated. In addition, the natural vibration frequency of OWT-MRE-TMD is reduced, compared with that of uncontrolled OWT. This is because the mass blocks of TMD increase the total mass of the wind turbine, leading to lower natural frequency.

The detailed comparison of acceleration amplitude reduction is listed in Table 4. For the tower top, the maximum amplitude are 13.97 dB and 4.13 dB for the first mode and second mode, and they are reduced by 74.73% (3.53 dB) and 0.24% (4.12 dB) by passive TMD. While with semi-active TMD, such two indexes are mitigated by 81.1% (2.64 dB) and 62.23% (1.56 dB), which demonstrates that semi-active TMD outperforms the passive TMD. Such phenomenon can be also found by the comparison of the maximum amplitude of tower base. It can be seen that semi-active TMD performs effectively not only for the first mode but for the second mode of the OWT structure.

Table 4. The amplitude (dB) of sweep acceleration response.

Systems	First mode		Second mode	
	Top	Base	Top	Base
Uncontrolled	13.97	2.802	4.13	10.49
Passive	3.53	0.685	4.12	10.11
Semi-active	2.64	0.501	1.56	4.56

4.2 Wind turbine under multi-hazard loadings

To examine the effectiveness of the MRE-TMD device, we considered two excitation conditions. Firstly, the combined wind and wave loadings are applied to the OWT structure, and these two excitations are in a period of 600s. Secondly, a multiple-hazard loading by wind, wave and seismic loadings are considered with two seismic excitations (e.g. the El-Centro excitation starts at 20s and ends at 73.8s, and Kobe starts at 30s and ends at 79.98s).

4.2.1 Combined wind and wave loadings

Figure 15 shows the time histories of the displacement at the OWT tower top and base with uncontrolled and controlled tower responses. The peak displacements of uncontrolled tower top and base are 0.9455 m and 0.1981 m respectively, and these responses reduced up to 59.24% and 57.29% by the variable stiffness MRE-TMD. It is shown that the MRE-TMD can significantly reduce the response.

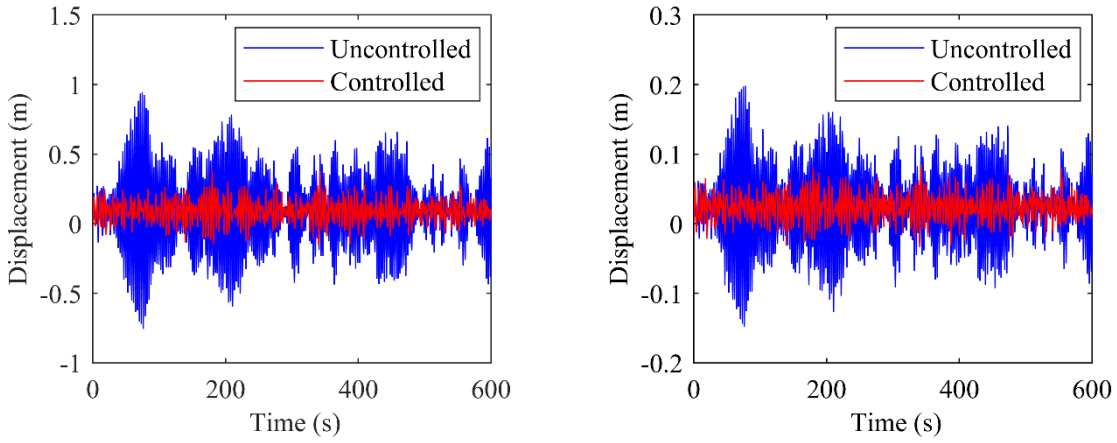

(a) (b)

Figure 15. Time histories of OWT displacement with and without MRE-TMD at different locations: (a) tower top, (b) tower base

To evaluate the effectiveness of the variable stiffness control, the displacement responses of wind turbine tower with passive TMD and semi-active MRE-TMD are listed in Table 5. Results confirm that, compared with passive TMD, semi-active TMD with variable stiffness exhibits better performance in attenuating excessive vibration in different locations of tower structure. The reduction by MRE-TMD for tower top is much obvious than that of tower base. This is reasonable because the combined wind and wave loadings excite the first fundamental vibration mode in which the maximum displacement occurred at tower top. When the semi-active MRE-TMD is applied, the reductions on RMS and peak of the displacement at tower top are 67.28% and 59.24%, and they are 49.49% and 57.29% at tower base.（参照 Ou.句式）

Table 5. Reduction in displacement responses of tower top and base with MRE-TMD

Systems	Tower top		Tower base	
	RMS	Peak value	RMS	Peak value
Uncontrolled	0.2784	0.9455	0.0584	0.1981
Passive	0.1447	0.4360	0.0332	0.1024
Semi-active	0.0911	0.3854	0.0295	0.0846

Figure 16 presents the single-sided spectrum of displacement amplitude and power spectrum density (PSD) of displacement at tower top. Excessive vibration is diminished in the excited resonance part near fundamental natural frequency under combined wind and wave loadings, especially by variable stiffness MRE-TMD. Although wind and wave loadings are low-frequency excitations, they are typical random excitations to induce the forced vibration of wind turbine structure. Hence, variable stiffness TMD perform better than the passive one. As shown in Figure 16, the reductions on peak of displacement amplitude spectrum and displacement PSD by variable stiffness MRE-TMD are 44.78% and 69.09%, compared with passive device.

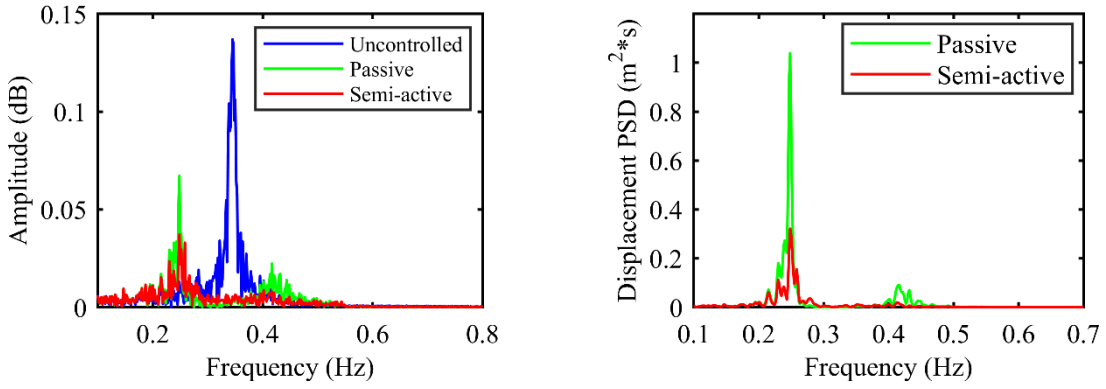

(a) (b)

Figure 16. Single-sided spectrum of tower top with and without MRE-TMD:
(a) displacement amplitude, (b) displacement PSD

Additionally, the stroke is an important index for the vibration device in wind turbine nacelle due to the limitation space. The stroke of passive TMD and MRE-TMD under wind and wave excitation are shown in Figure 17. It is desirable to obtain less stroke for reducing mis-functionality of control system. Compared with passive TMD, the peak stroke of MRE-TMD is reduced by 34.5% and RMS stroke is decreased by 40.2%. It is demonstrated that the use of semi-active MRE-TMD can obtain stronger energy absorption ability with less stroke.

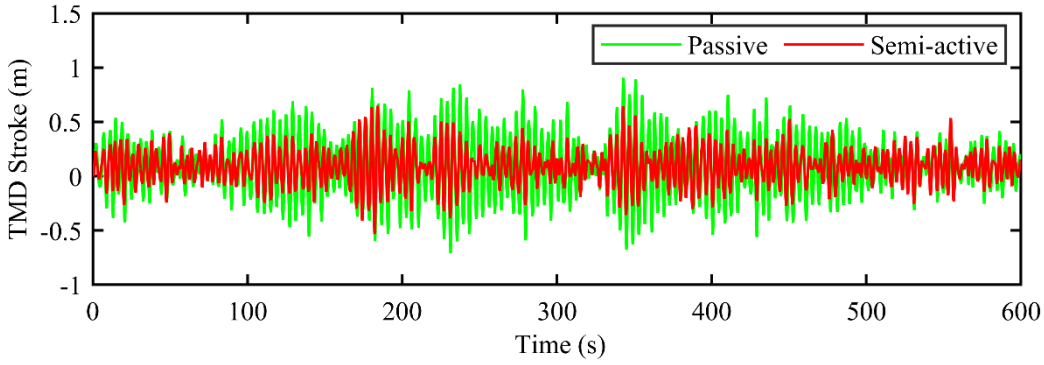

Figure 17. Stroke of passive TMD and MRE-TMD under wind and wave loadings

4.2.2 Combined wind, wave, and seismic loadings

Figure 18 shows the dynamic responses at tower top with passive TMD and MRE-TMD under different earthquakes. At the beginning of earthquake event (t=20 s in El-Centro and t=30 s in Kobe), the acceleration is obviously enlarged. Due to the low damping ratio of OWT (commonly less than or equal to 0.5%), the effect of seismic responses remains for about 130 s after the removal of the earthquake loading (El-Centro ends at 73.8s and Kobe ends at 79.98s). The same performance is also observed in Fitzgerald et al's work [], where the excessive responses by earthquake excitations remained dozens of seconds. In contrary to the OWT with passive TMD, the margin of acceleration responses by controllable MRE-TMD decay instantly, which shortens the time to normal responses after earthquake. By utilizing controlled MRE-TMD, the peak acceleration of tower top is reduced by 15.41% and 23.45% under Kobe and El-Centro, respectively.

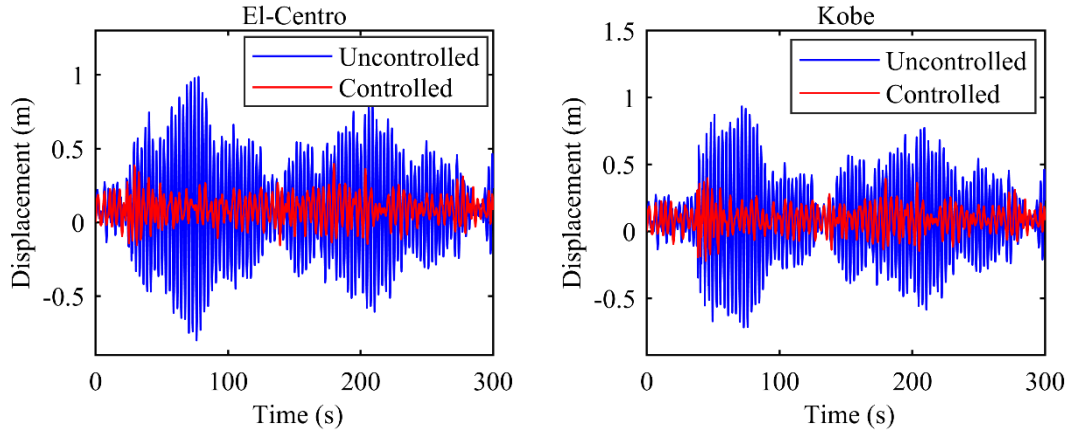

（a） (b)

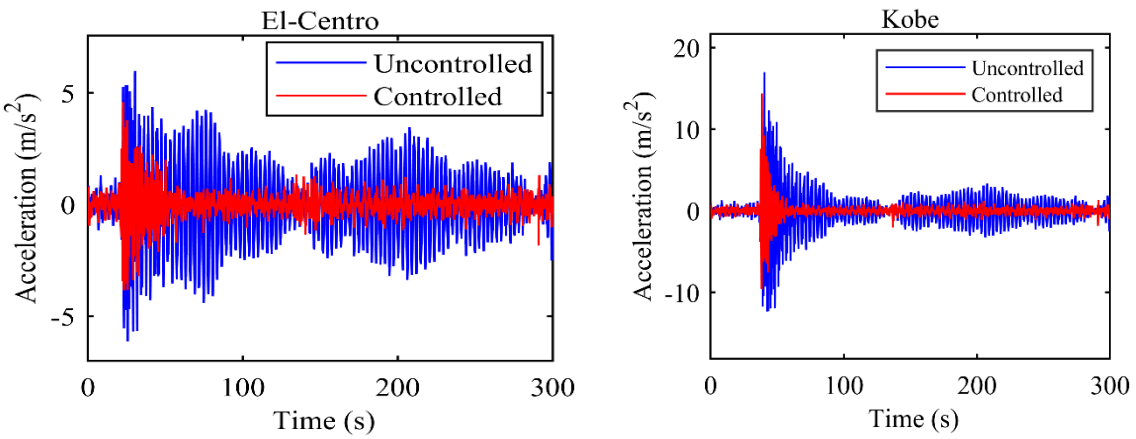

（c） (d)

Figure 18. Dynamic responses of tower top: (a) displacement time history in El-Centro, (b) displacement time history in Kobe, (c) acceleration time history in El-Centro and (d) acceleration time history in Kobe.

The distribution of the maximum lateral displacement of the turbine tower nodes are compared in Figure 19. It is shown that the lateral displacement distributes increasingly along the tower heights and variable stiffness MRE-TMD obviously reduces the maximum displacement. The inter-storey drift decreases in the tower structure, which is reasonable for the control effect of lateral displacement reduction gained using semi-active MRE-TMD. Especially, for the inter-storey drift from 3rd to 5th node along the tower, the peak displacement reductions are up to 20.1%, 53.65% and 60.05% under El-Centro earthquake, and 14.97%, 31.48% and 57.4% under Kobe earthquake.

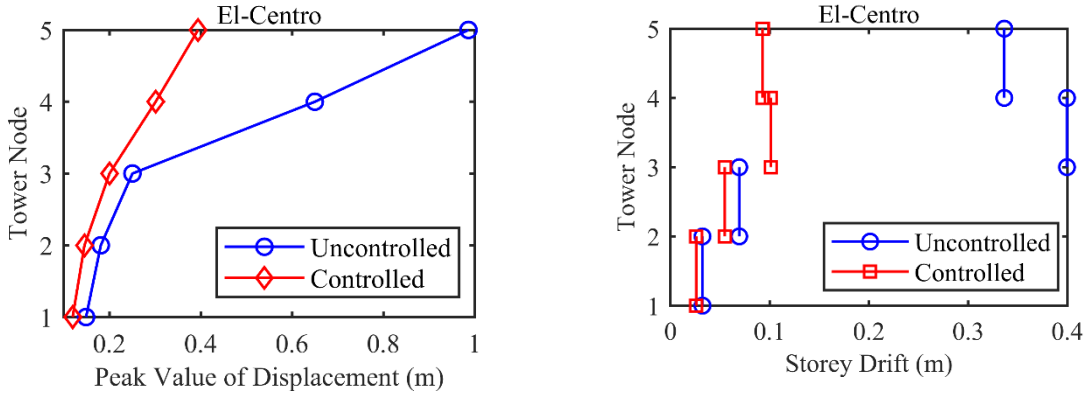

(a) (b)

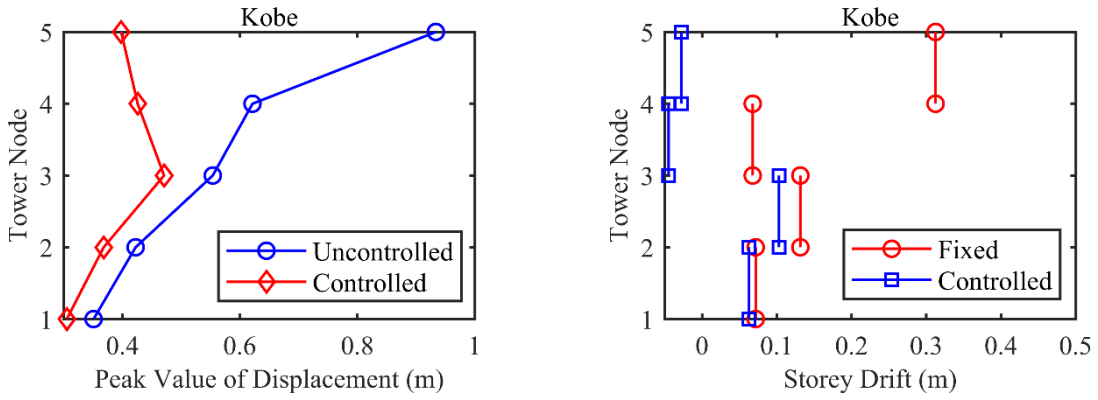

(c) (d)

Figure 19. Peak displacement value and storey drift of 5-DOFs above mean sea level

A comparison is presented in Table 6 for dynamic responses obtained from the controlled OWT under different strategies. The reductions in RMS on responses at tower top and base for passive TMD and semi-active MRE-TMD are shown. Based on the computed RMS value, it is observed that the reduction of displacement RMS are 39.17% and 44.77% on top of the tower and 8.29% and 30.11% on the base of the tower with respect to the OWT-passive-TMD structure by altering semi-active MRE-TMD due to El-Centro and Kobe earthquakes respectively. RMS acceleration at tower top and bas are decreased by 99.9% and 6.41% under El-Centro, and 99.96% and 34.65% under Kobe by using semi-active MRE-TMD, compared with passive TMD. It is concluded that the frequency-tracing algorithm performs better than passive one. The reason is that the passive TMD aimed at mitigation loading in a constant frequency near the first vibration mode; however, in the combined seismic loadings with wind and wave loadings, the second vibration mode of turbine structure is excited which is reflected by the following acceleration spectrum analysis, and thus the tuneable stiffness is superior.

Table 6. Reduction in RMS on dynamic responses of tower under different controlled states.

Earthquakes	Systems	RMS of top displacement	RMS of top acceleration	RMS of base displacement	RMS of base acceleration
El-Centro	Passive	0.1501	0.7401	0.0398	1.2797
	Semi-active	0.0913	0.0007	0.0365	1.1977
Kobe	Passive	0.1653	1.6346	0.0744	3.7922
	Semi-active	0.0913	0.0007	0.0520	2.4782

Additionally, as shown in Figure 20, applying semi-active MRE-TMD has largely reduced the stroke of TMD system as 70.18% and 74.32% under El-Centro and Kobe respectively compared with a passive TMD.

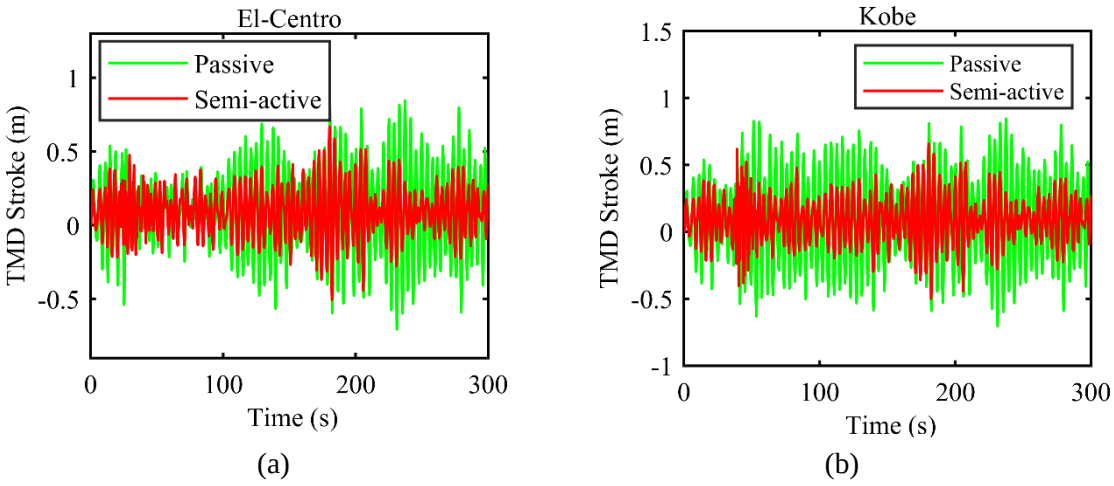

(a) (b)

Figure 20. Stroke of TMD and MRE-TMD: (a) El-Centro; (b) Kobe

Figure 21 shows acceleration amplitude of the tower top and base, and the obtained RMS of dynamic responses are compared in Table 7. According to Figure 21 (a) and (b), the second mode of tower top acceleration response is excited. The energy at the first vibration mode is significantly reduced, and the reductions on passive TMD and semi-active MRE-TMD are 81.31% and 91.61% under El-Centro respectively, and 70.11% and 86.96% under Kobe; for the second vibration mode, the reductions on semi-active MRE-TMD control are up to 45.53% and 70.41% under El-Centro and Kobe respectively, compared with 2.62% and 0.26% by passive TMD. Figures 21 (c) and (d) are the acceleration amplitude of the tower base where the maximum amplitude of the second mode shape occurs. The energy at the second vibration frequency mitigations under passive control and semi-active control are 5.1% and 10.27% for El-Centro earthquake, 2.85% and 56.98% for Kobe earthquake. The results demonstrate that the proposed semi-active MRE-TMD control strategy in present study can not only control the first mode response but also can obviously suppress the second mode of vibrations ([Using…]). This is reasonable because the frequency of acceleration response of tower top is applied as the tracing objective, which is a frequency sensitive signal. Additionally, although the second vibration mode occurs at the tower base, the acceleration response of tower is obvious as shown in Figure 18, which provides possibility to identify the high-mode frequency. However, due to the different characteristics of the seismic excitations [11, 46], the MRE-TMD is more feasible for near-fault Kobe than El Centro earthquake.

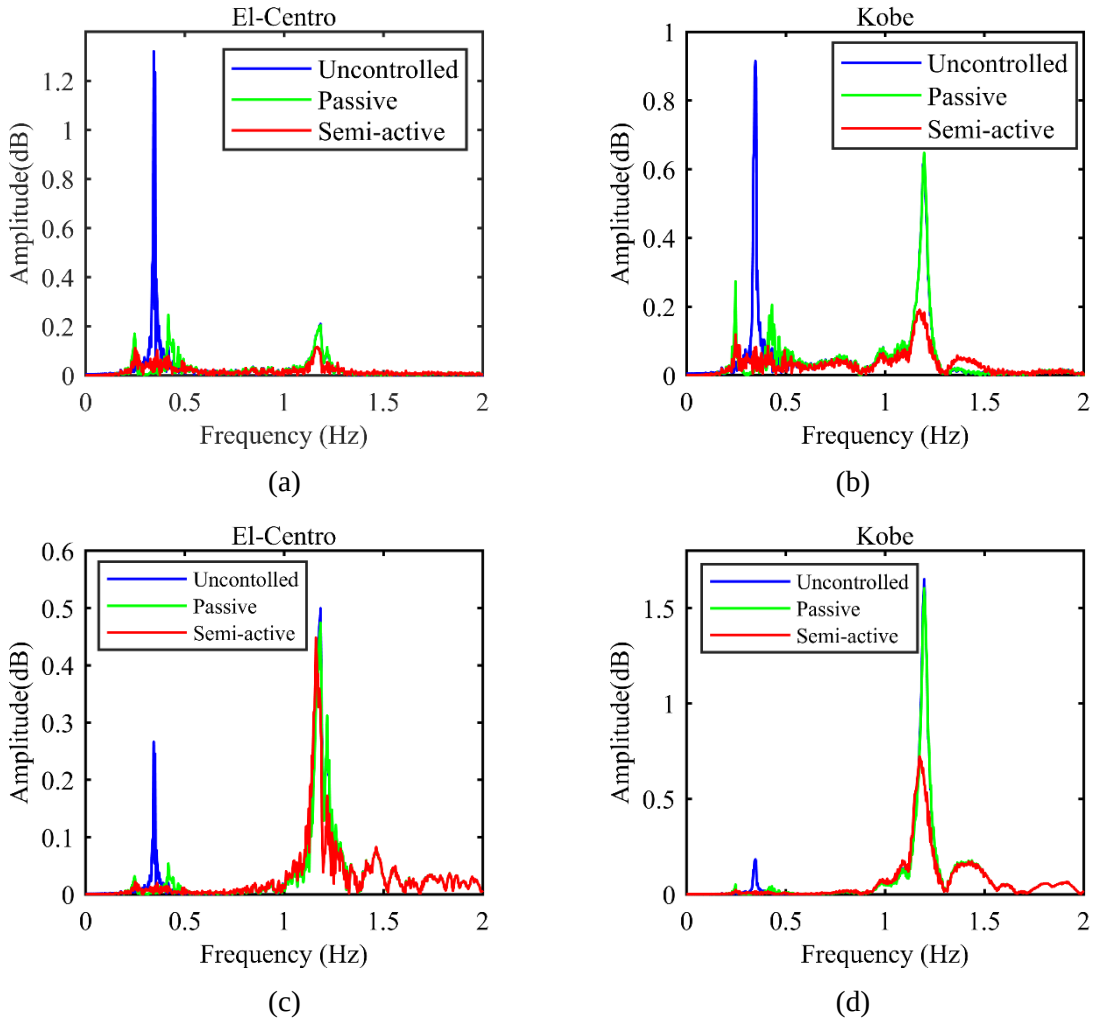

Figure 21. Acceleration amplitude (dB): (a, b) for the top and (c, d) for the base

Table 7. Acceleration amplitude (dB) of tower top and base

Earthquake	Systems	First mode		Second mode	
		Top	Base	Top	Base
El-Centro	Uncontrolled	1.32	0.2663	0.21	0.4996
	Passive	0.2467	0.0540	0.2045	0.4741
	Semi-active	0.1108	0.022	0.1144	0.4483
Kobe	Uncontrolled	0.9147	0.1832	0.6478	1.651
	Passive	0.2734	0.0517	0.6461	1.604
	Semi-active	0.1193	0.0236	0.1912	0.7102

4.3 Robustness control

Under the multi-hazard loadings, damage might occur to the foundation and the tower. Hence, the robustness control of the controlled MRE-TMD system for OWT considering damage is necessity. In this work, damage is considered through degrading the stiffness of the tower

structure. Three damage cases are considered: DC1, damage starts at 50s (before Kobe earthquake); DC2, damage starts at 120s (during earthquake); DC3, damage starts at 180s (after earthquake), all cases compared with no damage (ND) condition. A stiffness reduction of 5% [6] is introduced to represent the damage. Using frequency tracing STFT algorithm, the frequency of semi-active MRE-TMD can be retuned in real-time to match the varied dominant frequency of OWT structure due to stiffness decay, while the key parameters of passive TMD remain unchanged.

Figures 22-24 show the displacement time histories and spectrum amplitude of passive and semi-active control under different damage cases. Table 8 compares the RMS of displacement at tower top for different damage cases, and the reduction ratios by comparing semi-active MRE-TMD to passive TMD are also calculated.

Table 8. RMS of displacement for passive and semi-active under different damage cases

Type	Passive TMD	Semi-active MRE-TMD	Reduction (%)
ND	0.1734	0.0913	47.35
DC1	0.2323	0.1211	47.87
DC2	0.2370	0.1125	52.53
DC3	0.2044	0.1058	48.24

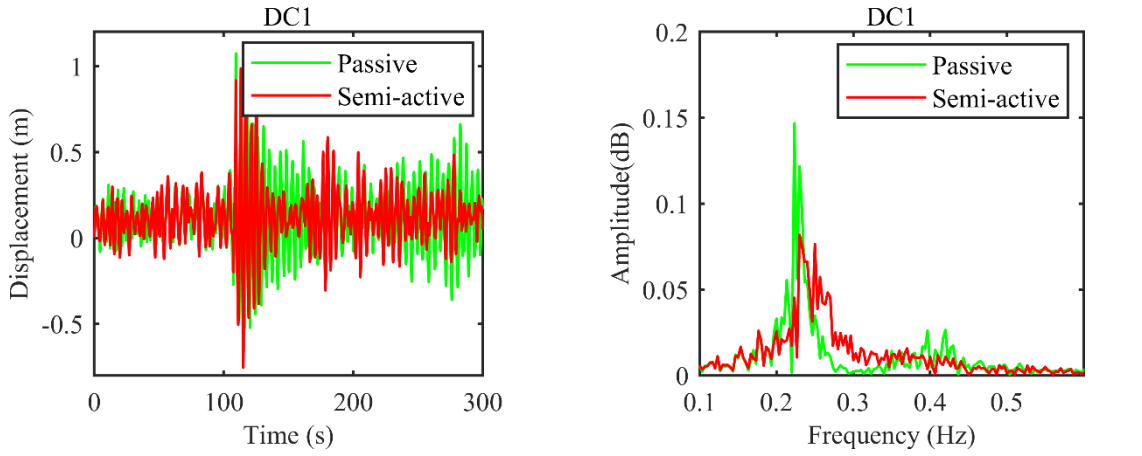

(a) (b)

Figure 22. Displacement time histories and amplitude (dB) of DC1:
(a) time histories and (b) amplitude for the top

In Table 8, when damage happens at 50s, it is found that the displacement peak of passive TMD at tower top is significantly increased by 33.97% compared with ND case, which indicates the passive TMD loses its effectiveness. To the contrary, the response controlled by the semi-active MRE-TMD remains a low level regardless of the damage and stiffness variation of OWT structure, and the maximum displacement by semi-active MRE-TMD is reduced to 30.16% compared with ND case. As shown in Figure 22, the response spectrum amplitude of OWT

with stiffness decay effect is also mitigated to a low level when the semi-active MRE-TMD is utilized.

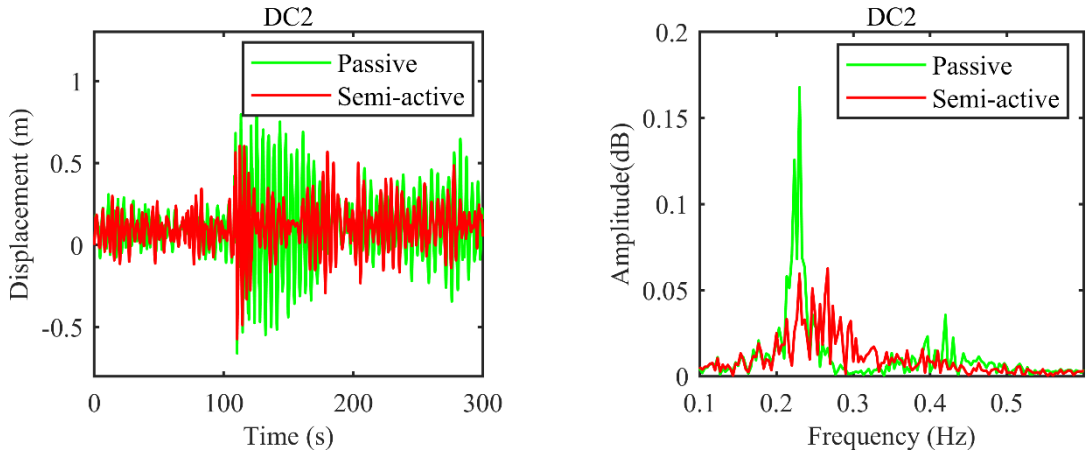

(a) (b)

Fig.23. Displacement time histories and amplitude (dB) of DC2:

(a) time histories and (b) amplitude for the top

Under DC2, the response results are shown in Figure 23 and Table 8. It is seen that the tower top displacement of passive TMD increased up to 36.68% compared to ND case, while the response amplitude remarkably reduced to a minimal level under semi-active MRE-TMD. Similar conclusions can be drawn under DC3 (in Figure 24 and Table 8), the response increase of passive TMD are 17.88%, and the peak value is still effectively mitigated when semi-active MRE-TMD is applied. Therefore, the MRE-TMD have better robustness on multi-mode vibration control and can effectively mitigate the response even under damage condition, which will prolong its fatigue life and reduce the potential maintenance cost.

(Damage 部分讨论参照 semi-active control of monopile offshore wind turbines under multi-hazards.)

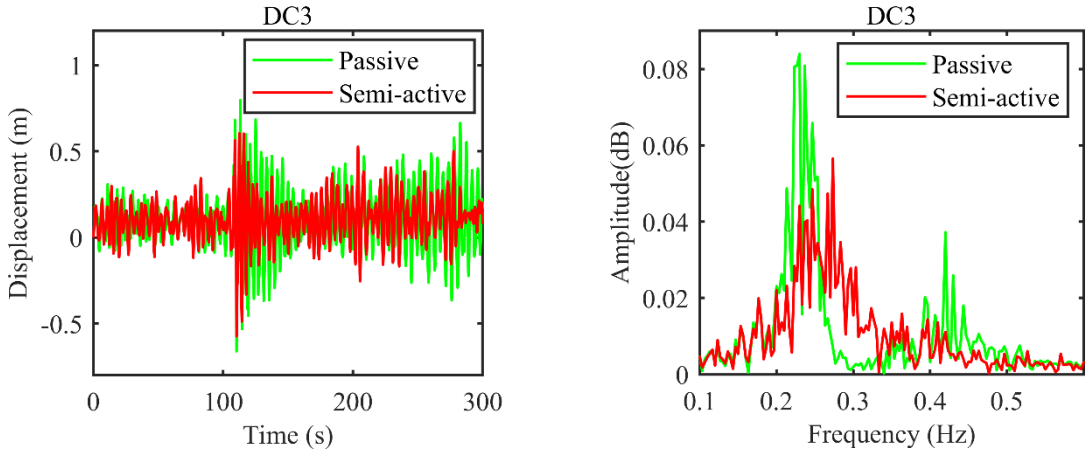

(a) (b)

Fig.24. Displacement time histories and amplitude (dB) of DC3:

(a) time histories and (b) amplitude for the top

5. Conclusions

This research focused on the vibration mitigation control of offshore wind turbine under combined wind, wave and seismic loadings using MRE-VSTMD. The design principle of proposed MRE-VSTMD is firstly presented. Using semi-active frequency-tracing algorithm, the stiffness of MRE can be tuned and the frequency of VSTMD is varied to the objective frequency of excited OWT structure. The feasibility of the proposed method has been evaluated and verified by numerical simulations. Some main conclusions are drawn as follows:

1. Semi-active MRE-VSTMD is suitable for multi-mode vibration control whereas passive TMD is mainly efficient for supressing first mode vibration.

2. Under combined wind and wave loadings, the controlled MRE-VSTMD can significantly reduce the peak displacement of OWT tower top and base by 59.24% and 57.29% respectively. Compared with passive TMD, semi-active MRE-TMD with variable stiffness exhibits better performance to attenuate excessive vibration in different locations of tower structure. In detail, the reductions on peak of displacement amplitude spectrum and displacement PSD by variable stiffness MRE-TMD are 44.78% and 69.09% of the passive TMD.

3. Under coupled wind, wave and earthquake loadings, the margin of acceleration responses of OWT top by controlled MRE-TMD decay instantly, which shortens the time to normal responses after earthquake. Compared with passive TMD, RMS displacement and acceleration responses are substantially decreased by semi-active TMD. In addition, the semi-active MRE-TMD achieves a smaller stroke than passive-TMD, which shows great advantage in practical application.

4. Under stiffness damage cases, MRE-TMD consistently shows effective control on the dynamic responses of OWT and presents strong robustness, which may be helpful to prolong the structure fatigue life and reduce the maintenance cost.

Acknowledgement

This work was supported by National Natural Science Foundation of China (No. 51709248).

Reference